


Rapidity dependence of nuclear coalescence: Impact on cosmic ray antinuclei

Kfir Blum*

Department of Particle Physics and Astrophysics, Weizmann Institute of Science, Rehovot, Israel (Received 2 October 2023; revised 3 February 2024; accepted 16 February 2024; published 27 March 2024)

Upcoming studies at the CERN Large Hadron Collider (LHC) aim to extend the rapidity coverage in measurements of the production cross section of antinuclei \bar{d} and $\overline{{}^3\text{He}}$. I illustrate the impact of such studies on cosmic ray (CR) flux predictions, important, in turn, for the interpretation of results from CR experiments. I show that, in terms of the rapidity effect, covering the range $|y| < 1.5$ at the LHC should be sufficient for the astrophysical CR calculation. Important extrapolation remains in other aspects of the problem, notably, \sqrt{s} .

DOI: [10.1103/PhysRevC.109.L031904](https://doi.org/10.1103/PhysRevC.109.L031904)

Introduction and results. Secondary astrophysical antimatter is produced in the galaxy in a fixed-target setup with high-energy primary cosmic rays (CRs, mostly p) scattering on ambient gas (mostly p). Detecting this astrophysical flux (already achieved for \bar{p} and e^+) is one of the main goals of CR experiments [1,2]. The production cross sections for antimatter particles formed in pp collisions are not calculable from first principles and must be obtained from accelerator experiments. A general obstacle is the limited kinematical coverage of these experiments (see, e.g., Refs. [3–5]). This becomes particularly important for antinuclei like \bar{d} and $\overline{{}^3\text{He}}$. Reference [3] demonstrated the impact of p_t and \sqrt{s} coverage for \bar{p} , \bar{d} , and $\overline{{}^3\text{He}}$ production (see the Appendix in Ref. [3]), but the rapidity dependence was not exhibited. Reference [5] discussed \bar{p} production kinematics, including rapidity (or Feynman x), but did not consider \bar{d} and $\overline{{}^3\text{He}}$. This Letter illustrates the impact of rapidity coverage on antinuclei production, anticipating experimental progress [6].

At the time of writing, accelerator yields of \bar{d} and $\overline{{}^3\text{He}}$ have only been reported for $|y| < 0.475$ [7–11]. However, the prediction of the CR flux arising from hadronic collisions is obtained by integration over all kinematical configurations leading to a given CR energy, including kinematical regions that fall outside of the measured range in rapidity. The theoretical prediction is therefore based to some extent on extrapolation. A simple way to assess the extent of the extrapolation is by setting the differential production cross section to zero in the relevant kinematical region and inspecting the impact on the flux. The calculation is reviewed in the body of this Letter; here, to show the motivation for the analysis, I fast forward to the main result, summarized by Fig. 1.

In each panel of Fig. 1, dealing with \bar{p} , \bar{d} , and $\overline{{}^3\text{He}}$, different curves show the CR flux that is obtained when in the kinematical integration of the CR yield the differential cross

section is set to zero outside of a certain range in rapidity, noted in the legend. The widths of the bands in the plot reflect the experimental uncertainty on the coalescence factors [12] from Refs. [7,8,10,11] and do not include other uncertainties, of which the dominant ones are due to the nucleonic (\bar{p}) cross section (of the order of 10–20% [3,4]) and astrophysical propagation in the galaxy (again roughly 10–20%, provided that the calculation is restricted to relativistic CRs with magnetic rigidity $\mathcal{R} = p/eZ$ of a few gigavolts and above, and assuming that the main propagation effect is calibrated using measurements of heavier secondary CRs like the boron/carbon flux ratio [13]).

Note the following two lessons from Fig. 1, focusing on \bar{d} and $\overline{{}^3\text{He}}$.

- (i) At rigidity $\mathcal{R} \lesssim 5$ GV, about 90% of the CR \bar{d} and $\overline{{}^3\text{He}}$ flux predictions hinges on extrapolation. The effect is less substantial near $\mathcal{R} \approx 10$ GV and becomes prominent again at $\mathcal{R} \gtrsim 100$ GV.
- (ii) CERN Large Hadron Collider (LHC) experiments could essentially close the rapidity gap if they provide antinuclei yields covering the range $|y| < 1.5$. (Note that the astrophysical CR \bar{d} flux at $\mathcal{R} > 100$ GV may be very challenging to measure, regardless of cross-section details.)

Even with rapidity effects settled, it is important to stress that LHC experiments in collider mode¹ are mostly limited to very high $\sqrt{s} \approx$ a few TeV, while the bulk of CR \bar{d} are the product of pp collisions at $\sqrt{s} < 30$ GeV. For example, the analysis in Appendix A in Ref. [3] (see Fig. 7 therein) shows that for CR at $\mathcal{R} = 10$ GV only about 6%, 15%, and 30% of \bar{p} , \bar{d} , and $\overline{{}^3\text{He}}$, respectively, come from initial states with $\sqrt{s} > 25$ GeV. In this important sense, the CR calculation is rooted in extrapolation, regardless of rapidity. Nevertheless,

¹But see the fixed-target programs of Refs. [14,15] and, notably, the low- \sqrt{s} experiments of the AMBER [16] and NA61/SHINE [17] Collaborations.

*kfir.blum@weizmann.ac.il

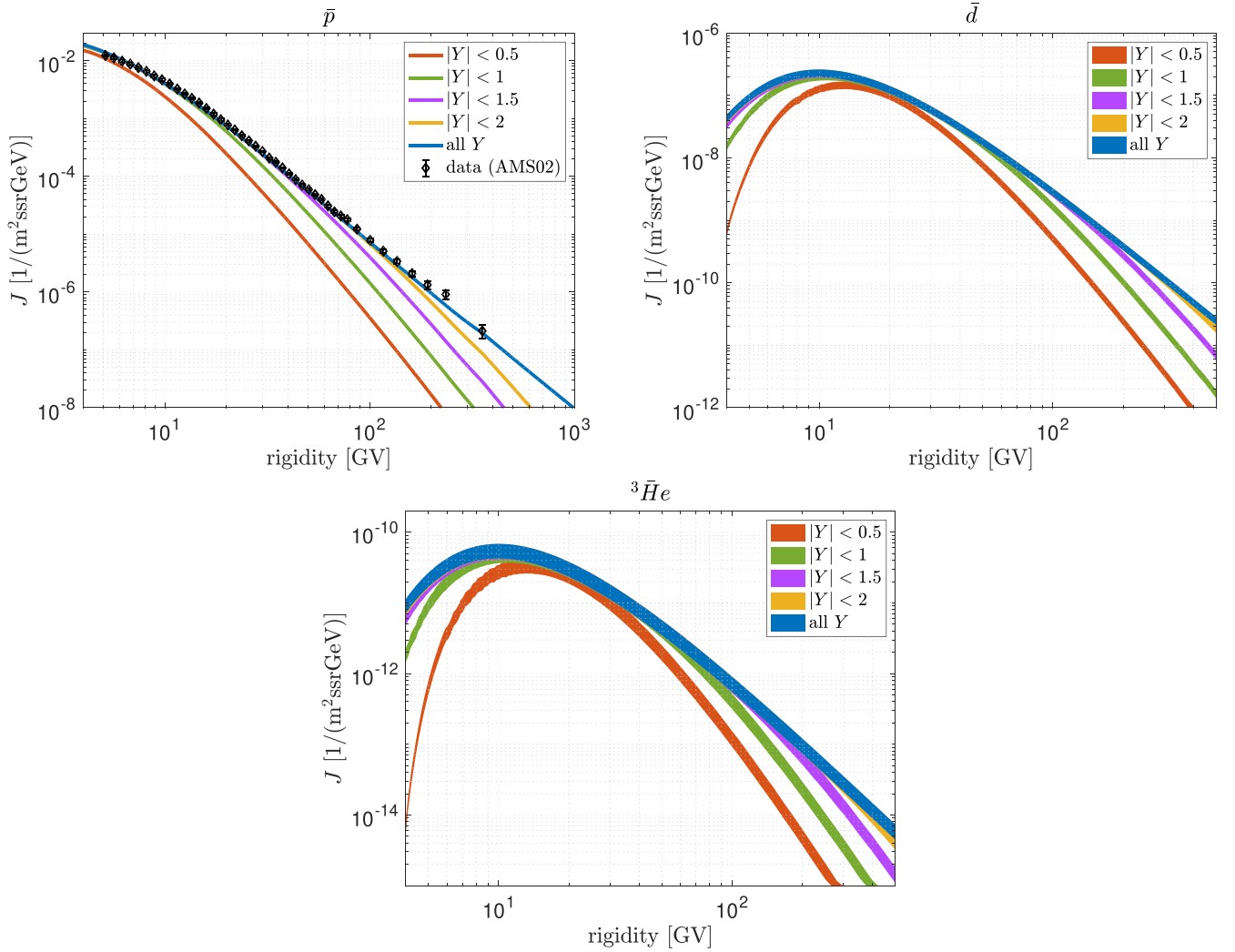


FIG. 1. Impact of rapidity cut on predicted CR antinuclei fluxes.

it would obviously be reassuring to see at least the high- \sqrt{s} region of the production cross section brought under control.

Outline of the calculation. The production rate density of antinucleus species a ($a = \bar{d}$ and ${}^3\bar{\text{H}}e$) in the galaxy per unit column density of the interstellar matter (ISM) target, via pp collisions, is given by [3]²

$$Q_a^{pp}(\mathcal{R}) = \frac{1}{m} \int_{\epsilon_a}^{\infty} d\epsilon_p n_p(\epsilon_p) \frac{d\sigma_{pp \rightarrow a}(\epsilon_p, \epsilon_a)}{d\epsilon_a}. \quad (1)$$

Up to small corrections from nuclear binding energies, the final-state rigidity \mathcal{R} (the convenient quantity when dealing with CR propagation) is related to the final-state energy via $Z^2 \mathcal{R}^2 = \epsilon_a^2 - A^2 m_p^2$, where A and Z are the mass and charge numbers. The integral is performed over ϵ_p , the observer frame energy of the incoming primary proton, with primary proton number density $n_p(\epsilon_p)$. The mean ISM target nucleon

mass is $m \approx 1.3m_p$. The observer frame energy of the product is ϵ_a . The key object is the Lorentz-invariant differential cross section ($\epsilon_a \frac{d\sigma_{pp \rightarrow a}}{d^3\mathbf{p}_a}$), which enters as

$$\frac{d\sigma_{pp \rightarrow a}(\epsilon_p, \epsilon_a)}{d\epsilon_a} = 2\pi p_a \int dc_\theta \left(\epsilon_a \frac{d\sigma_{pp \rightarrow a}}{d^3\mathbf{p}_a} \right). \quad (2)$$

Here, $p_a = |\mathbf{p}_a|$ is the magnitude of the observer frame three-momentum of a , and θ is the observer frame scattering angle. The transverse momentum is $p_{at} = p_a s_\theta$. I abbreviate $c_\theta = \cos \theta$ and $s_\theta = \sin \theta$.

As far as astrophysics is concerned, it would be desirable to receive direct accelerator measurements of ($\epsilon_a \frac{d\sigma_{pp \rightarrow a}}{d^3\mathbf{p}_a}$) in as many kinematic configurations as possible. In practice, one attempts to reduce the required kinematics coverage by using a coalescence prescription [12,18,19],

$$\left(\epsilon_a \frac{d\sigma_{pp \rightarrow a}}{d^3\mathbf{p}_a} \right) = R_A(\tilde{\epsilon}_X) B_A(\mathbf{p}_p) \left(\epsilon_{\bar{p}} \frac{d\sigma_{pp \rightarrow \bar{p}}}{d^3\mathbf{p}_{\bar{p}}} \right)^A. \quad (3)$$

²For ${}^3\bar{\text{H}}e$, one needs to add the contribution of \bar{t} which decays in flight and is produced with a similar cross section [11].

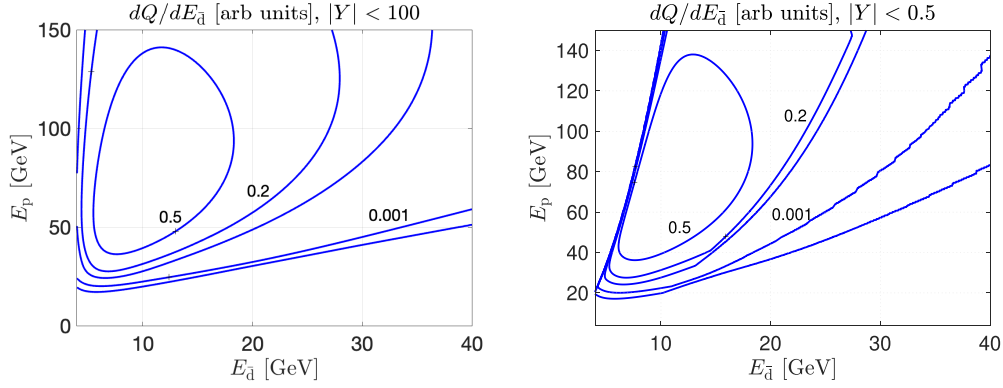


FIG. 2. Proton flux-weighted, p_{at} -integrated differential cross section for \bar{d} production. (a) No rapidity cut. (b) Nulling kinematic regions with $|y| < 0.475$.

Here, $B_A(\mathbf{p}_p)$ is the coalescence factor, and the prescription is useful if $B_A(\mathbf{p}_p)$ is a slow-varying function of the kinematics. $R_A(\tilde{\epsilon}_X)$ is a phase-space correction factor (see Appendix C of Ref. [3]). $\tilde{\epsilon}_X$ is the energy of the residual state produced in association with a in the reaction $pp \rightarrow aX$: $\tilde{\epsilon}_X = \sqrt{s + m_a^2} - 2\sqrt{s}\tilde{\epsilon}_a$, defined in the pp center-of-mass (c.m.) frame, where $\tilde{\epsilon}_a$ is the energy of a in the c.m. frame and

$$s = 2m_p(m_p + \epsilon_p) \quad (4)$$

is the pp collision center-of-mass energy. ($\epsilon_p \frac{d\sigma_{pp \rightarrow \bar{p}}}{d^3\mathbf{p}_p}$) is the Lorentz-invariant production cross section for antiprotons, for which the kinematical coverage of accelerator data is usually much better than that for antinuclei. I use the parametrization from Ref. [4], calibrated on LHC and other data sets.

In Fig. 1, in the \bar{d} calculation, the baseline value of the coalescence factor B_2 is taken from ALICE pp analysis at $\sqrt{s} = 7$ TeV [7].³ For ${}^3\text{He}$, the baseline value of B_3 is taken from Refs. [10,11].⁴ Note yet again that the uncertainty bands in Fig. 1 only include the experimental measurement uncertainties on B_A .

Impact of a rapidity cut. The rapidity of a is defined in the c.m. frame as $y = \frac{1}{2} \ln \frac{\tilde{\epsilon}_a + \tilde{p}_{az}}{\tilde{\epsilon}_a - \tilde{p}_{az}} = \frac{1}{2} \ln \frac{1 + \tilde{\beta}_z}{1 - \tilde{\beta}_z}$, so the c.m. frame longitudinal boost velocity is $\tilde{\beta}_z = \tanh y$. The boost factor between the observer frame and the c.m. frame is

$$\gamma = \frac{\sqrt{s}}{2m_p} = \sqrt{\frac{m_p + \epsilon_p}{2m_p}}. \quad (5)$$

The observer frame boost factor to the rest frame of a is $\gamma_a = \frac{\epsilon_a}{m_a} = \frac{1}{\sqrt{1 - \tilde{\beta}_a^2}}$, with which $p_a = \beta_a \epsilon_a = \gamma_a \beta_a m_a = m_a \sqrt{\gamma_a^2 - 1}$. The c.m. frame energy of a , $\tilde{\epsilon}_a$, is $\tilde{\epsilon}_a = m_a(\gamma\gamma_a - c_\theta\sqrt{\gamma^2 - 1}\sqrt{\gamma_a^2 - 1})$. Using $\tilde{p}_{az}^2 = \tilde{\epsilon}_a^2 - p_a^2 s_\theta^2 -$

m_a^2 , one finds

$$\begin{aligned} \tilde{\beta}_z &= \sqrt{1 - \frac{p_a^2 s_\theta^2 + m_a^2}{\tilde{\epsilon}_a^2}} \\ &= \sqrt{1 - \frac{1 + (\gamma_a^2 - 1)s_\theta^2}{(\gamma\gamma_a - c_\theta\sqrt{\gamma^2 - 1}\sqrt{\gamma_a^2 - 1})^2}}. \end{aligned} \quad (6)$$

An experimental cut $|y| < Y$ implies that in the CR production calculation, the regions of the integrals over ϵ_p and θ , which deviate outside of the restriction [where $\gamma = \gamma(\epsilon_p)$ via Eq. (5)]

$$1 - \frac{1 + (\gamma_a^2 - 1)s_\theta^2}{(\gamma\gamma_a - c_\theta\sqrt{\gamma^2 - 1}\sqrt{\gamma_a^2 - 1})^2} < \tanh^2 Y, \quad (7)$$

are based on extrapolation. As noted earlier, one can assess to what extent the astrophysics CR computation depends on extrapolation, by setting to zero the part of the integration which goes outside of the tested kinematic region. This is the method used to implement the rapidity cuts in Fig. 1.

There is a convenient approximate way to inspect the kinematics constraints in the ϵ_a, ϵ_p plane, glossing over the θ (or p_a) variable. To get there, let us first plot the integrand of Eq. (1),

$$\frac{dQ_a^{pp}(\epsilon_p, \epsilon_a)}{d\epsilon_p} = n_p(\epsilon_p) \frac{d\sigma_{pp \rightarrow a}(\epsilon_p, \epsilon_a)}{d\epsilon_a}. \quad (8)$$

In this definition I drop an overall constant factor and consider the result in arbitrary units. The result for $a = \bar{d}$ is shown in Fig. 2. In Fig. 2(a), I show the full result without a rapidity cut. In Fig. 2(b), I show the result restricted to the region $|y| < 0.475$. To understand the physical significance of this plot, recall that the astrophysics source term at observer frame a energy ϵ_a is obtained⁵ by integrating $\frac{dQ_a^{pp}(\epsilon_p, \epsilon_a)}{d\epsilon_p}$ over ϵ_p , the y axis of the plot. The nulled regions in Fig. 2(b) show how swaths of ϵ_p contributing to the integral are based

³ALICE pp analysis at $\sqrt{s} = 13$ TeV [8] finds consistent, but slightly lower B_2 .

⁴ALICE pp analysis at $\sqrt{s} = 7$ TeV [9] finds consistent, but slightly higher B_3 .

⁵Up to an uninteresting propagation effect.

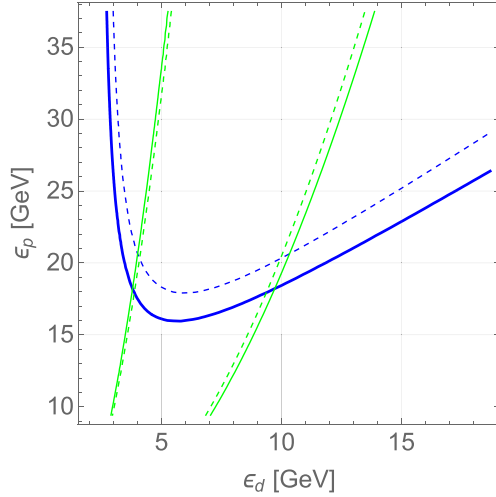


FIG. 3. Kinematics and rapidity regions for \bar{d} production. The generally allowed kinematic region is above the blue solid line (in the direction of the dashed line). The region $|y| < 0.475$ is between the green solid lines (in the direction of the dashed line).

on cross-section extrapolation. Removing high-rapidity kinematic regions is seen to suppress production at both low and high ϵ_a .

The Appendix contains similar plots including also \bar{p} and ${}^3\text{He}$, as well as corresponding plots that show the p_t -integrated differential cross section without weighing it by the proton flux (that is, $\frac{d\sigma_{pp \rightarrow a}(\epsilon_p, \epsilon_a)}{d\epsilon_a}$).

The general shape of the differential source term is understood by considering the maximal energy available for a in the c.m. frame:

$$\tilde{\epsilon}_a < \frac{4m_p^2\gamma^2 + m_a^2 - M_X^2}{4m_p\gamma}, \quad (9)$$

where M_X is the minimal invariant mass of the residual hadronic state produced in association with a . (For example, if $a = \bar{d}$, the minimal reaction product is $pp \rightarrow \bar{n}\bar{p}pppn$, so the residual hadronic state must contain at least four nucleons and $M_X \approx 4m_p$. Similarly, for $a = {}^3\text{He}$, the minimal reaction is $pp \rightarrow \bar{n}\bar{p}\bar{p}ppppn$, and $M_X \approx 5m_p$.)

In Fig. 3, above the solid blue contour Eq. (9) is satisfied, and below it, it is not. This blue contour delineates the general shape of the differential source in Fig. 2(a): near the edge of the region, this source is shaped essentially by phase space.

The rapidity coverage can now be easily understood approximately by noting that most of the secondary production occurs not far from the forward region, $c_\theta \approx 1$. Setting $c_\theta = 1$ and $s_\theta = 0$ in Eq. (7), I plot the contour $\tanh^2 y = \tanh^2 Y$ (with Y being the rapidity cut) by the green line in Fig. 3. Between the green lines (in the direction of the dashed line), Eq. (7) is satisfied. This approximate consideration (glossing over the p_t or θ integral) explains the shape of Fig. 2(b).

Treatment of CR propagation. To make Fig. 1, I followed Ref. [3] in computing the antinuclei CR flux with and without rapidity cuts. The calculation of predicted antinuclei flux uses the measured flux of CR nuclei to calibrate the rigidity-dependent mean column density of CRs [20]. A good fit to the B/C flux ratio measured by the AMS02 experiment in the range $4 \text{ GV} \lesssim \mathcal{R} \lesssim 10^3 \text{ GV}$ is provided by

$$X_{\text{esc}} \approx 10.475 \left(\frac{\mathcal{R}}{10 \text{ GV}} \right)^{-0.4756} \times \left[1 + \left(\frac{\mathcal{R}}{3 \times 10^3 \text{ GV}} \right)^{0.6} \right] \text{ g/cm}^2. \quad (10)$$

The differential number density of relativistic ($\mathcal{R} \gg 1 \text{ GV}$) antinuclei is then predicted via

$$n_a(\mathcal{R}) \approx \frac{Q_a(\mathcal{R})X_{\text{esc}}(\mathcal{R})}{1 + \frac{\sigma_a}{m}X_{\text{esc}}(\mathcal{R})}, \quad (11)$$

where σ_a is the inelastic cross section for antinucleus-ISM collisions. The source term Q_a is a sum of different production channels, including proton-proton and proton-helium collisions: $Q_a = Q_a^{pp} + Q_a^{p\text{He}} + Q_a^{\text{He}p}$. All are proportional to the same underlying pp cross section and are affected by the rapidity dependence of B_A in approximately the same way.

For \bar{p} , the prediction can be compared to measured data, shown in the top left panel of Fig. 1.

More model-dependent calculations of CR propagation are often used in the literature. These details are not essential for the impact of rapidity coverage, and one expects other astrophysical model calculations to reach conclusions similar to those reached here.

Summary. Progress in cosmic ray (CR) measurements in space [2] makes the prediction of CR antimatter fluxes very timely. This comes at fantastic coincidence with the LHC program [6]. I clarified the importance of rapidity coverage in the experimental measurements of antinuclei production cross sections (p_t and \sqrt{s} coverage was discussed in Ref. [3]). The main result is that extending the range of rapidity coverage at the LHC to $|y| > 0.475$ is essential for CR antinuclei predictions. Covering the range $|y| < 1.5$ would settle the predictions of CR \bar{d} and ${}^3\text{He}$ to good accuracy.

Even with rapidity effects settled, it is important to note that LHC experiments in collider mode are mostly limited to very high $\sqrt{s} \approx$ a few TeV, while the bulk of CR \bar{d} are the product of pp collisions at $\sqrt{s} < 30 \text{ GeV}$ (see Appendix A in Ref. [3]). In this important sense, the CR calculation is rooted in extrapolation even after the rapidity effects are settled at high \sqrt{s} . This issue is a central goal for the fixed-target programs of Refs. [14–17].

Acknowledgments. I am grateful to Chiara Pinto and Alberto Caliva for pointing out the relevance of the CR production rapidity analysis for the LHC program at ALICE. This work was supported by the Israel Science Foundation under Grant No. 1784/20.

APPENDIX: ADDITIONAL KINEMATIC PLOTS

Figure 4 repeats the information presented in Fig. 2, extending it to \bar{p} and $\overline{^3\text{He}}$. Figure 5 extends these results to the anti-nuclei source without weighing by the CR proton flux.

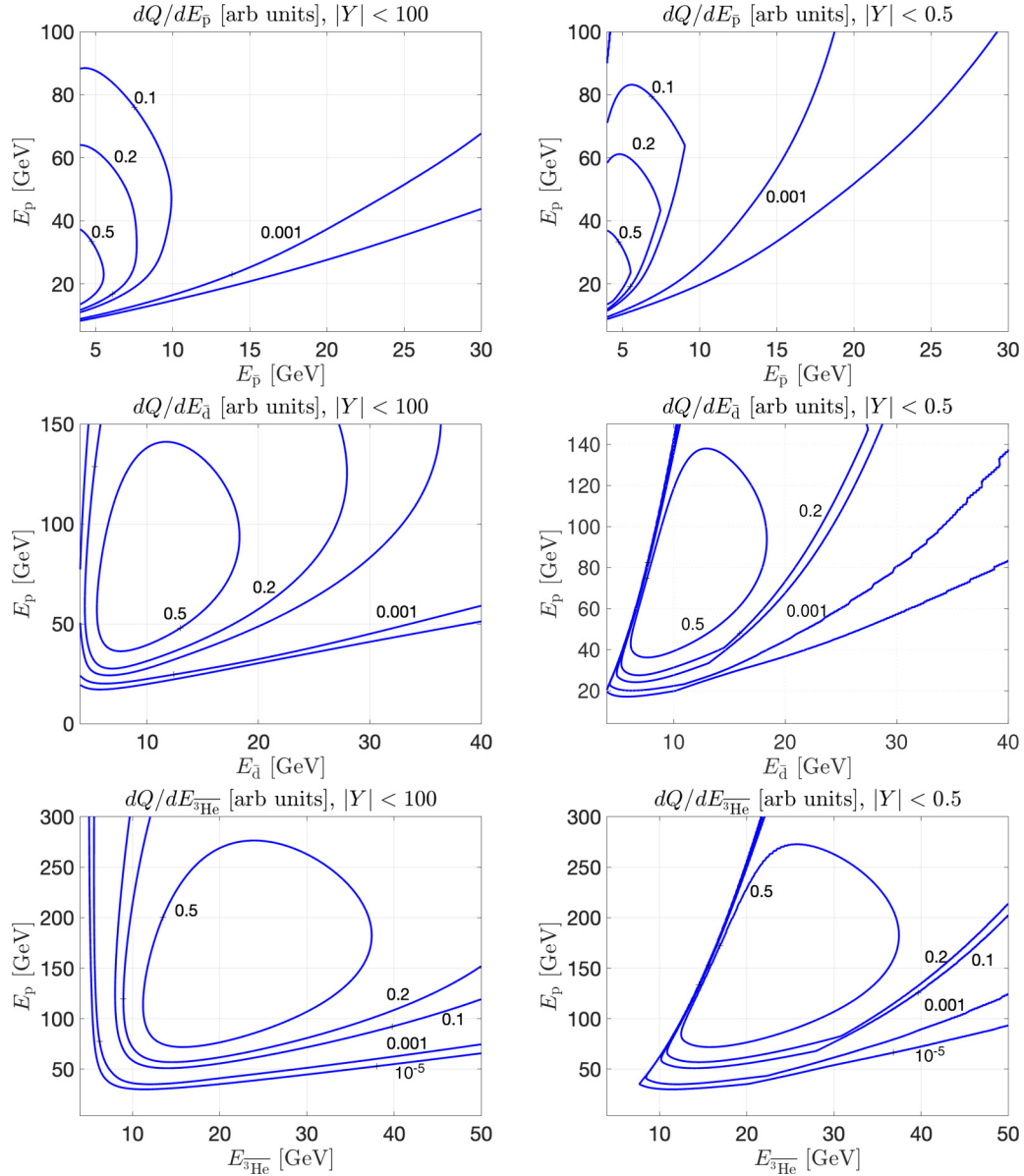


FIG. 4. Proton flux-weighted, p_{at} -integrated differential cross section for \bar{p} (top panels), \bar{d} (middle panels), and $\overline{^3\text{He}}$ (middle panels) production. Left panels: No rapidity cut. Right panels: Nulling kinematic regions with $|y| < 0.475$.

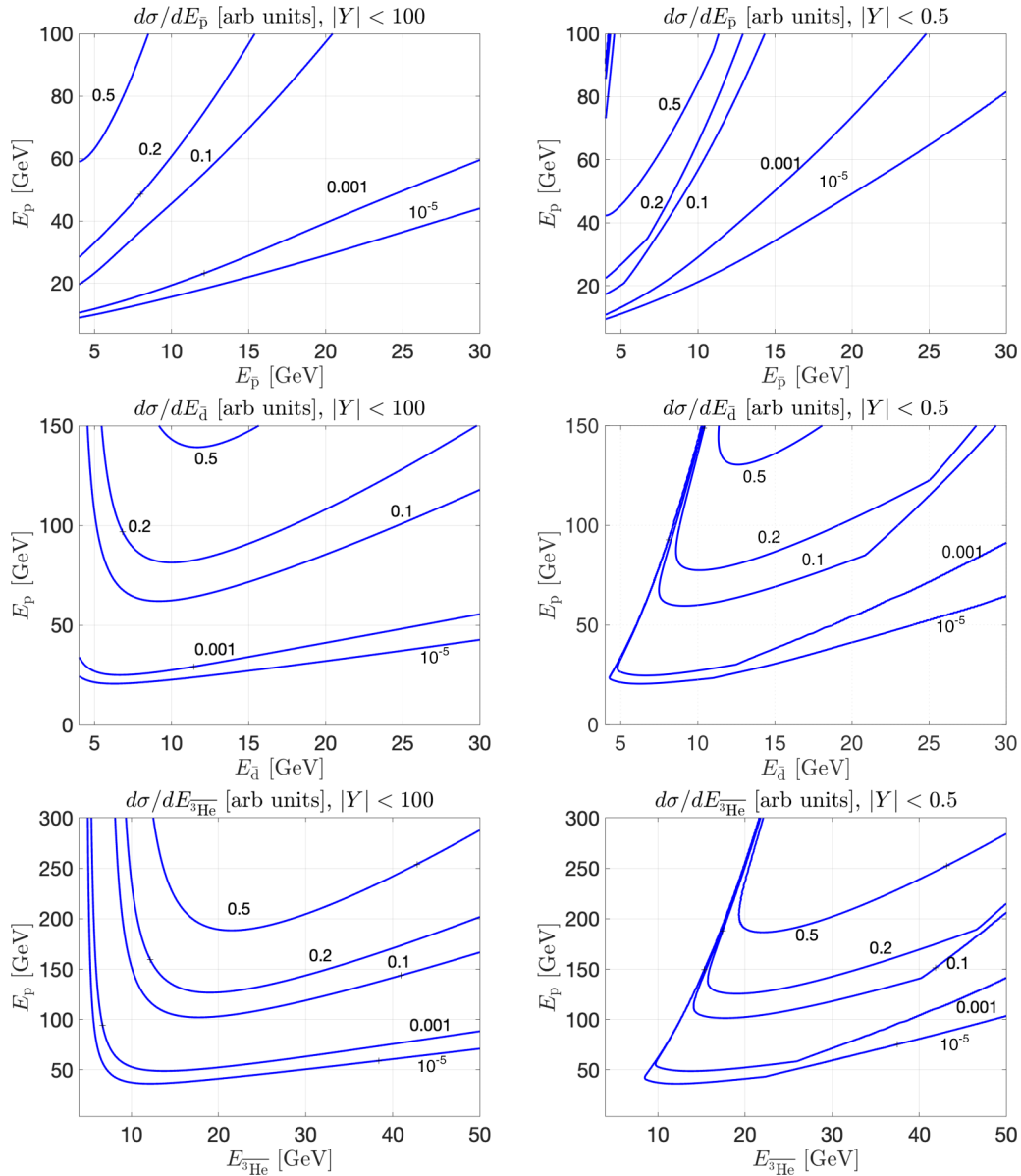


FIG. 5. p_{at} -integrated (not proton-flux weighted) differential cross section for \bar{p} (top panels), \bar{d} (middle panels), and $\bar{^3\text{He}}$ (middle panels) production. Left panels: No rapidity cut. Right panels: Nulling kinematic regions with $|y| < 0.475$.

- [1] M. Simon (PAMELA Collaboration), *AIP Conf. Proc.* **1516**, 239 (2013).
- [2] J. Berdugo (AMS Collaboration), *Moscow Univ. Phys.* **77**, 71 (2022).
- [3] K. Blum, K. C. Y. Ng, R. Sato, and M. Takimoto, *Phys. Rev. D* **96**, 103021 (2017).
- [4] K. Blum, R. Sato, and M. Takimoto, *Phys. Rev. D* **98**, 063022 (2018).
- [5] M. Korsmeier, F. Donato, and M. Di Mauro, *Phys. Rev. D* **97**, 103019 (2018).
- [6] Z. Citron *et al.*, CERN Yellow Rep. Monogr. **7**, 1159 (2019).
- [7] S. Acharya *et al.* (ALICE Collaboration), *Phys. Lett. B* **794**, 50 (2019).
- [8] S. Acharya *et al.* (ALICE Collaboration), *Eur. Phys. J. C* **80**, 889 (2020).
- [9] S. Acharya *et al.* (ALICE Collaboration), *Phys. Rev. C* **97**, 024615 (2018).
- [10] S. Acharya *et al.* (ALICE Collaboration), *Eur. Phys. J. C* **82**, 289 (2022).
- [11] S. Acharya *et al.* (ALICE Collaboration), *J. High Energy Phys.* **01** (2022) 106.
- [12] F. Bellini, K. Blum, A. P. Kalweit, and M. Puccio, *Phys. Rev. C* **103**, 014907 (2021).
- [13] K. Blum, R. Sato, and E. Waxman, [arXiv:1709.06507](https://arxiv.org/abs/1709.06507).
- [14] D. Kikoła *et al.* (AFTER@LHC study), *Nucl. Phys. A* **982**, 971 (2019).

- [15] C. Hadjidakis *et al.*, PoS **HardProbes2018**, 041 (2019).
[16] B. Seitz, PoS **ICHEP2022**, 839 (2023).
[17] A. Marcinek (NA61/SHINE Collaboration), *Acta Phys. Pol. B Proc. Suppl.* **16**, 1 (2023).
[18] R. Scheibl and U. W. Heinz, *Phys. Rev. C* **59**, 1585 (1999).
[19] K. Blum and M. Takimoto, *Phys. Rev. C* **99**, 044913 (2019).
[20] B. Katz, K. Blum, and E. Waxman, *Mon. Not. R. Astron. Soc.* **405**, 1458 (2010).